

PSFC/JA-09-12

## Observations of Electromagnetic Fields and Plasma Flow in Hohlräume with Proton Radiography

**C. K. Li<sup>1</sup>, F. H. Séguin<sup>1</sup>, J. A. Frenje<sup>1</sup>, R. D. Petrasso<sup>1</sup>,  
P. A. Amendt<sup>2</sup>, O. L. Landen<sup>2</sup>, J. R. Rygg<sup>2</sup>, R. P. J.  
Town<sup>2</sup>, R. Betti<sup>3,4</sup>, J. P. Knauer<sup>3</sup>, D. D. Meyerhofer<sup>3,4</sup>,  
J. M. Soures<sup>3</sup>, C. A. Back<sup>5</sup>, D. Kilkenny<sup>5</sup>, and A. Nikroo<sup>5</sup>**

<sup>1</sup>*Plasma Science and Fusion Center, Massachusetts Institute of Technology,  
Cambridge, Massachusetts 02139, USA*

<sup>2</sup>*Lawrence Livermore National Laboratory, Livermore, California 94550 USA*

<sup>3</sup>*Laboratory for Laser Energetics, University of Rochester, Rochester, New York  
14623, USA*

<sup>4</sup>*Department of Mechanical Engineering, Physics and Astronomy, University of  
Rochester, Rochester, New York 14623, USA*

<sup>5</sup>*General Atomics, San Diego, California 92186 USA*

22 April 2009

Plasma Science and Fusion Center  
Massachusetts Institute of Technology  
Cambridge, MA 02139 USA

The work was performed at the LLE National Laser User's Facility (NLUF), and was supported in part by US DOE (DE-FG52-07NA28059 and DE-FG52-06N826203), LLNL (B543881 and LDRD-ER 898988), and LLE (414090-G), The Fusion Science Center at University of Rochester (412761-G).

Accepted for publication in *Physical Review Letters*

---

# Observations of electromagnetic fields and plasma flow in hohlraums with proton radiography

C. K. Li, F. H. Séguin, J. A. Frenje, and R. D. Petrasso

*Plasma Science and Fusion Center, Massachusetts Institute of Technology, Cambridge, Massachusetts 02139, USA*

P. A. Amendt, R. P. J. Town, O. L. Landen, and J. R. Rygg

*Lawrence Livermore National Laboratory, Livermore, California 94550 USA*

R. Betti\*, J. P. Knauer, D. D. Meyerhofer\*, and J. M. Soures

*Laboratory for Laser Energetics, University of Rochester, Rochester, New York 14623, USA*

C. A. Back, J. D. Kilkenny, and A. Nikroo

*General Atomics, San Diego, California, 92186 USA*

We report on the first proton radiography of laser-irradiated hohlraums. This experiment, with vacuum gold (Au) hohlraums, resulted in observations of self-generated magnetic fields with peak values  $\sim 10^6$  Gauss. Time-gated radiographs of monoenergetic protons with discrete energies (15.0 and 3.3 MeV) reveal dynamic pictures of field structures and plasma flow. Near the end of the 1-ns laser drive, a stagnating Au plasma ( $\sim 10 \text{ mg cm}^{-3}$ ) forms at the center of the hohlraum. This is a consequence of supersonic, radially directed Au jets ( $\sim 1000 \text{ } \mu\text{m ns}^{-1}$ ,  $\sim \text{Mach 4}$ ) formed as laser-driven plasma bubbles approach one another.

**PACS numbers: 52.38.Fz, 52.30.-q, 52.57.-z, 52.50.Jm**

A high- $Z$  enclosure, *i.e.*, hohlraum, creates an environment filled with a nearly blackbody (Planckian) radiation field when irradiated by high-power lasers or energetic ions [1,2]. The cavity generates intense thermal x rays at a radiation temperature ( $T_r$ ) of hundreds of eV. Hohlraums have been extensively used as radiation sources or platforms for a wide range of basic and applied physics experiments. In studies of laboratory astrophysics and high-energy-density (HED) physics [3,4], for example, hohlraums are used for creating and simulating various extreme HED conditions, including those of stellar and planetary interiors. The hohlraum radiation field is used to compress spherical capsules, through capsule ablation, to high temperature and density in indirect-drive inertial confinement fusion (ICF) [1,2].

The use of hohlraums requires an understanding of physics details, such as coupling efficiency, plasma conditions, instabilities, radiation uniformity [1,2,5,6] and cavity shape [1,2,7,8]. Any electric ( $E$ ) or magnetic ( $B$ ) fields generated within a hohlraum may have important effects on overall performance [9].  $B$  fields inside a hohlraum can reduce heat flow, since cross-field thermal conductivity is modified by a factor of  $(1 + \omega_{ce}^2 \tau^2)^{-1}$ , where  $\omega_{ce}$  is the electron gyro frequency and  $\tau$  is the collision time [10,11].  $E$  fields may modify the plasma conditions and, if sufficiently large, could enhance thick-target bremsstrahlung at x-ray energies well above the Planckian background. Such fields could alter distributions of electron temperature ( $T_e$ ) and density ( $n_e$ ), affecting laser-plasma instabilities and drive uniformity.

For low-intensity laser drive, such as used in most hohlraum experiments [1-9], the dominant source for  $B$ -field generation is expected to be non-parallel electron density and temperature gradients ( $\nabla n_e \times \nabla T_e$ ) [10,11]. The  $E$  field is expected to result from electron pressure gradients ( $\nabla P_e$ ) [10,11]. Despite such expectations, prior to this work, no direct experimental measurement and characterization of such hohlraum fields have been made.

The first observations of  $E$  and  $B$  fields and their evolution in hohlraums, made with time-gated monoenergetic proton radiography [12], are presented in this Letter. Coupled plasma flow dynamics were also observed. Simultaneous imaging with two discrete proton energies (3.3 and 15 MeV) breaks any inherent degeneracy between  $E$  and  $B$ . These measurements reveal new physical phenomena and provide a previously unavailable test for validating 3-dimensional (3D) radiation-hydrodynamic and kinetic codes [13].

The experiments, illustrated schematically in Fig. 1, were performed at the OMEGA laser facility [14]. The proton sources were  $\text{D}^3\text{He}$ -filled, thin-glass-shell targets driven by 21 OMEGA laser beams, producing a  $\sim 130$ -ps-long pulse of protons; the relative timing of backlighter and subject hohlraum drive was adjusted [12] to sample the hohlraum at a desired time. The proton radiographs were recorded using CR-39 detectors [15], and the isotropy of the backlighter allows two different experiments to be performed simultaneously in each shot (Fig. 1a). The hohlraums were of the OMEGA scale-1.5 size [1] with 30- $\mu\text{m}$ -thick gold walls, 100% laser entrance holes (LEH), 2.4-mm diameter, and 2-mm length. Each hohlraum was driven by 10 laser beams (incidence angle  $58.8^\circ$ ) forming a single irradiation ring with total laser energy  $\sim 4 \text{ kJ}$  in a 1-ns square pulse. The individual laser beams had full spatial and temporal smoothing [16]. SG4 phase plates resulted in each beam illuminating an elliptical spot on the wall with a ratio of long-to-short axis  $\sim 1.2$  and laser intensity  $\sim 2 \times 10^{14} \text{ W cm}^{-2}$ . A nickel mesh (60  $\mu\text{m}$  thick, 150- $\mu\text{m}$  hole-to-hole spacing, and 75- $\mu\text{m}$  square holes) [12] divided backlighter protons into discrete beamlets to allow quantitative measurement of proton trajectory displacements due to fields.

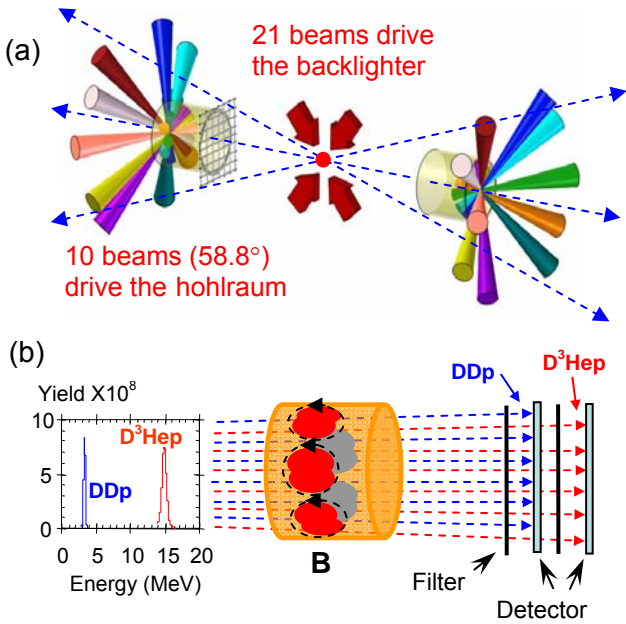


FIG. 1. (Color) Experimental setup (a), with proton backlighter, subject hohlraums, and laser beams. The distance between the backlighter and the mesh (detector) was 0.7 (27) cm. Typical energy spectrum and “sandwich-like” detector are shown in (b). The filters and the thickness of the front detector were carefully chosen so that 3.3-MeV DD protons were recorded only on that detector while 15-MeV D<sup>3</sup>He protons were recorded only on the second detector [18].

Figure 2 shows sequences of proton images obtained on three different shots, covering a time period from the beginning of the laser pulse ( $t = 0$  ns) to 0.8 ns after it was off ( $t \approx 1.8$  ns). At earlier times ( $t \leq 0.9$  ns) the beamlet arrays in 15-MeV images (Fig 2a) show minimal displacement by fields or plasma, but beamlets have different sizes at different times, reflecting more subtle

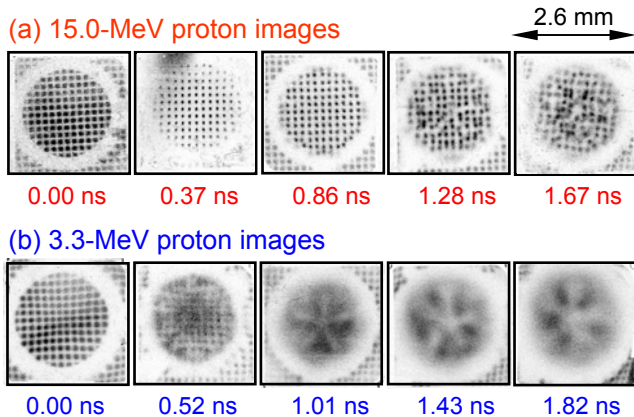


FIG. 2. (Color online) Radiographs of a 10-laser-beam driven Au hohlraum at different times, taken with 15.0-MeV D<sup>3</sup>He protons (a), and 3.3-MeV DD protons (b), illustrating spatial structure and time evolution of proton deflection and beamlet size (within each image, darker means higher fluence). The corresponding pairs of the images in (a) and (b) were taken in the same shot, but give different sample times due to different proton velocities. The gray-scale mapping of the image display is different in each image to account for the different backlighter yields and to make the most important structures clearly visible.

field effects. At late times the 15-MeV beamlets show some chaotic spatial structure, indicating that their trajectories have been affected by large field and plasma effects. In the 3.3-MeV images (Fig. 2b), beamlet arrays are coherently distorted by  $t = 0.52$  ns and disappear altogether (due to stronger deflections) at later times.

Angular deflection of each beamlet is proportional to both  $\int \mathbf{B} \times d\mathbf{l}$  and  $\int \mathbf{E} \times d\mathbf{l}$  (where  $d\mathbf{l}$  is the differential pathlength along the proton trajectory), and can be determined from  $\xi$ , the linear displacement of a beamlet in an image from the position it would have had in the absence of deflections (in this Letter we use the apparent size of the displacement scaled to the imaged subject). For certain situations with enough symmetry, the potential degeneracy between  $E$  and  $B$  can be broken [17,18]. Here this is overcome by near-simultaneous 3.3 and 15 MeV radiographs. Because of the Lorentz force, deflections due to  $B$  are inversely proportional to the square root of proton energy ( $\xi \propto \epsilon_p^{-1/2}$ ) while those due to  $E$  are inversely proportional to proton energy ( $\xi \propto \epsilon_p^{-1}$ ). Measuring beamlet displacements in images from a single shot with these distinct proton energies (ignoring small flight time differences) breaks the degeneracy. Neither experiment nor simulation, performed as described here but with a single particle energy, can unequivocally separate the effects of  $E$  and  $B$  fields.

The lineouts in Fig. 3 show that the beamlets are approximately uniformly spaced in the hohlraum center region for both 15-MeV (Fig. 3a) and 3.3-MeV protons (Fig. 3b), but that they expand, by different amounts in the proximity of the hohlraum wall. The displacements are estimated to be  $\approx 30$   $\mu\text{m}$  for 15-MeV protons and  $\approx 75$   $\mu\text{m}$  for 3.3-MeV protons. These displacements have a ratio  $75/30 \sim 2.5$ , which is close to the square root of the energy ratio  $(15/3.3)^{1/2} \approx 2.2$  expected from  $B$ -field

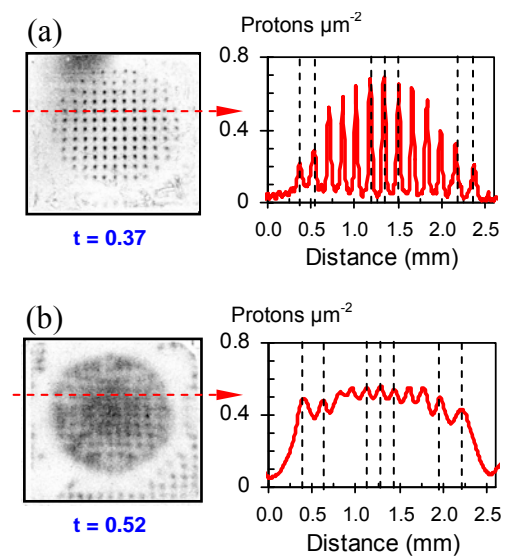


FIG. 3. (Color online) Lineouts indicate that the arrays of beamlets are slightly expanded in proximity to the hohlraum wall; displacements  $\xi \sim 30$   $\mu\text{m}$  and  $\sim 75$   $\mu\text{m}$  for 15-MeV (a) and 3.3-MeV (b) protons, respectively.

deflection, but far from the energy ratio  $(15/3.3) \approx 4.6$  expected from  $E$ -field deflections. This comparison suggests that the  $B$  field is the dominant source for the observed proton deflections near the hohlraum wall.

Estimating the absolute magnitude of  $B$  field involves consideration of the proton trajectories near the hohlraum wall, where they encounter two regions of  $B$  field with opposite signs,  $\mathbf{B}_1$  and  $\mathbf{B}_2$ , as they pass through the two sides of a laser-generated bubble. The deflections in the two regions don't quite cancel because the trajectories of the protons are not exactly parallel to the axis of the hohlraum, so  $\delta B \equiv |\mathbf{B}_2 - \mathbf{B}_1|$  is not zero. We can infer  $\delta B$  from the net beamlet displacement using the formula  $\delta B \propto \xi \varepsilon_p^{1/2} L_B^{-1}$  [12], where  $L_B \sim L_T \equiv T_e (\nabla T_e)^{-1}$  is the temperature scale length which is about the radius of the plasma bubble ( $\sim 200 - 400 \mu\text{m}$ ). Using either  $\xi \sim 30$  (for  $\varepsilon_p = 15 \text{ MeV}$ ) or  $\xi \sim 75 \mu\text{m}$  (for  $\varepsilon_p = 3.3 \text{ MeV}$ ) implies  $\delta B \sim 0.1 \text{ megaGauss (MG)}$ . To estimate  $B$  from  $\delta B$ , we use a result from a 2D LASNEX radiation-hydrodynamic simulation [19], which indicates that  $\delta B/B \sim 0.1$ ; whence it follows that  $B \sim 1 \text{ MG}$ .

Electrical charging of the hohlraum, which is electrically connected to the Ni mesh, is indicated by the apparent hole-size reduction seen most clearly in the 15 MeV radiograph at 0.37 ns and the lineout plotted in Fig. 4a (symmetry requires that this apparent constriction is an  $E$ -field effect). The  $E$ -field must be associated with gradients in the electrical potential around the mesh holes (on the incoming side only, since the hohlraum acts as a Faraday cage). It can be estimated from a simple formula based on the experimental geometry:  $E \approx 4\varepsilon_p q^{-1} L_E^{-2} \Delta$ , where  $\Delta \approx 0.5A(D-\varpi)L_E a^{-1}(A-a+L_E)^{-1}$  is the apparent displacement at the mesh plane;  $D$  is the mesh hole spacing ( $75 \mu\text{m}$ );  $\varpi$  is the width (FWHM) of the lineout at the mesh plane;  $a$  ( $A$ ) is the distance from backlighter to mesh (detector);  $q$  is the proton charge; and  $L_E$  is the field scale length. Protons see a transverse field mainly as they enter a mesh hole, and the scale length along their trajectory is about the transverse size of the hole, or  $75 \mu\text{m}$ . The field estimates for different times are plotted in Fig. 4b, showing that a peak  $E$  field  $\sim 2 \times 10^9 \text{ V m}^{-1}$  occurs at  $\sim 0.37 \text{ ns}$ . Interestingly, the field decays away, a likely consequence of discharging, even while the laser drive is on (Fig 4b). Similar charging and discharging effects

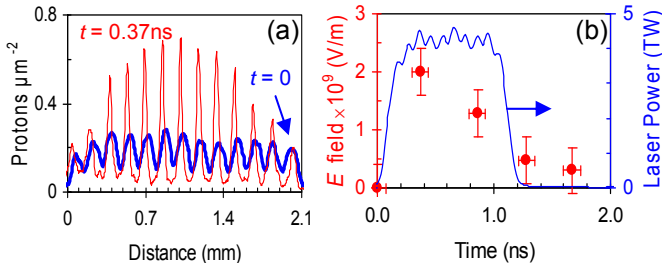


FIG. 4 (Color) (a) Lineouts from 15-MeV images of  $t = 0.0$  and  $0.37 \text{ ns}$ , shown in Fig. 2a. The characteristic widths  $\varpi$  (FWHM) are the measure of the beamlets on the mesh plane. (b)  $E$  fields estimated from experimental measurements (solid circles).

have been seen for (arbitrary) targets irradiated by lasers of this intensity. It is this effect that, for thin-glass-shell targets of the experiments described herein and elsewhere [20], caused a slight upshift in the nuclear fusion birth energy from 3.0 (14.7) MeV to 3.3 (15.0) MeV.

A striking feature in Fig. 2 is a 5-prong asterisk-like fluence pattern in the 3.3-MeV proton images at  $t \geq 1.01 \text{ ns}$  and later [21,22]. As illustrated in Fig. 5, such an asterisk is a direct consequence of the staggered distribution of laser beams on the hohlraum wall. Although all are incident at  $58.8^\circ$  to the normal, the ten laser beams are grouped to form five pairs with  $26.8^\circ$  between two beams within each pair, but  $45.2^\circ$  between adjacent pairs (Fig. 5a). For the experimental conditions ( $T_e \sim 1 \text{ keV}$ ,  $T_i \sim 1 \text{ eV}$ , and  $n_e \sim 0.1n_c$ ), the plasmas have a high  $\beta$  ( $\equiv 8\pi n_e k T_e B^{-2} \sim 10-100$ ) and a sound speed [ $C_s \sim (ZT_e m_i^{-1})^{1/2} \sim 200 - 300 \mu\text{m ns}^{-1}$ ] that sets a scale for hydrodynamic expansion [23]. With  $\sim 200 \mu\text{m}$  between pairs of bubbles (Fig. 5a), it is expected that adjacent bubbles should coalesce in  $\sim 0.35 \text{ ns}$  and reach the hohlraum axis in  $\sim 3 - 4 \text{ ns}$ . In contrast the 3.3 MeV radiograph at 1.01 ns indicates, on the basis of the 5-prong asterisk pattern extending to the axis, that Au-plasma jets shoot inward at about  $\sim \text{Mach } 4$  ( $\sim 1000 \mu\text{m ns}^{-1}$ ). The subsequent 3.3-MeV radiograph at 1.43 ns shows a much more enhanced asterisk pattern. A faint outline of the same asterisk pattern is shown on the corresponding 15-MeV radiograph (at 1.28 ns). From this latter set of radiographs (Fig. 5c), the width of the proton-fluence depletion region in a leg of the asterisk is  $\sim 50$  ( $260$ )  $\mu\text{m}$  for the 15 (3.3) MeV protons. If depletion is a

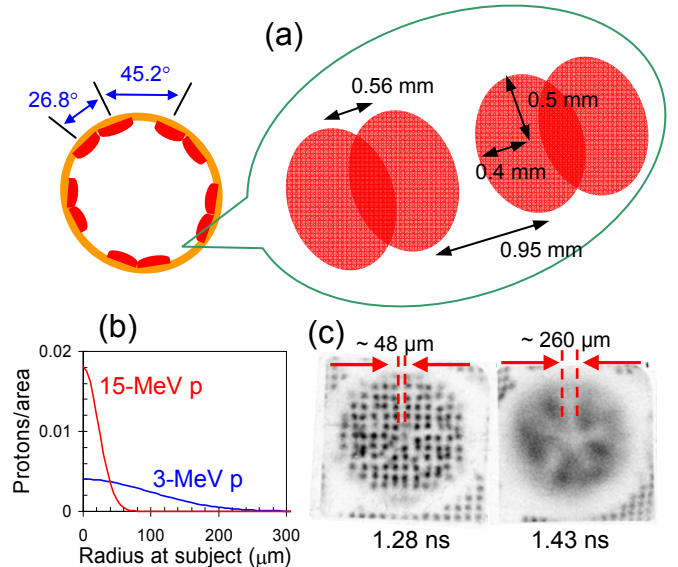


FIG. 5. (Color online) Carton to illustrate laser beam distribution in OMEGA Cone 3 configuration (a). Calculated proton scattering distributions at subject plane for a  $\sim 1 \text{ mg cm}^{-2}$  Au plasma (b) It is shown that, the scattering width (FWMH) for 3-MeV protons is  $235 \mu\text{m}$ , while scattering width (FWMH) for 15-MeV protons is  $52 \mu\text{m}$ . These estimates are comparable with the measured widths (c) of the stagnating plasma ( $\sim 260 \mu\text{m}$  and  $\sim 48 \mu\text{m}$ , respectively).

result of scattering off the Au plasma, its density can be estimated. Figure 5b shows the effects of scattering calculated for 3.3 and 15 MeV protons in a  $1 \text{ mg cm}^{-2}$  Au plasma. As the scattering width varies inversely with the proton energy [24], the 3.3 MeV scattering profile is broader by about a factor 5. The observations (Fig 5c) for both the 3.3 and 15 MeV protons are consistent with  $1 \text{ mg cm}^{-2}$  Au areal density [25, 26]. Taking the scale size for the Au plasma (in the direction of the hohlraum axis) to be  $\sim 1 \text{ mm}$ , the Au density is  $\sim 10 \text{ mg cm}^{-3}$ .

To explore aspects of these intrinsic 3D phenomena, highly-resolved 1D LASNEX radiation-hydrodynamic simulations were run with the Au-plasma bubble expanding into an ultra-low density vacuum. These simulations indicate an expansion rate almost comparable to the jets. In addition to this pure hydrodynamic expansion, the hot electrons advancing ahead of the rarefaction expansion could further boost the motion of the Au ions by the ion sound speed [27]. Work is in progress to assess whether such a hybrid motion of the Au bubble is sufficient to generate a nearly  $10 \text{ mg cm}^{-3}$  stagnation density on the symmetry axis by  $\sim 1 \text{ ns}$ .

In summary, we report on the first observations of self-generated fields associated with laser-irradiated hohlraums. Time-gated radiographs of monoenergetic protons with discrete energies (15.0 and 3.3 MeV) reveal a dynamic picture of field structure during and after the laser drive. Discrete but disparate monoenergetic proton energies enable discrimination between  $E$  and  $B$  fields. Peak  $B$  fields were  $\sim 10^6$  Gauss. Gold plasma ( $\sim 10 \text{ mg cm}^{-3}$ ) stagnates on the hohlraum axis by 1 ns due to  $\sim$  Mach 4 ( $v \sim 1000 \text{ } \mu\text{m ns}^{-1}$ ) jets that form between adjacent laser-generated plasma bubbles. (Note that this should not occur in an ignition hohlraum, where a gas fill would impede the jets.) These experimental results have important implications for understanding the precise conditions and plasma dynamics inside vacuum hohlraums and provide an impetus for the further development of 3D multi-fluid codes with self-consistent field generation.

The authors thank Dr. L. J. Suter and Dr. S. H. Glenzer of LLNL for useful discussions. The work was performed at the LLE National Laser User's Facility (NLUF), and was supported in part by US DOE (DE-FG52-07NA28059 and DE-FG52-06N826203), LLNL (B543881 and LDRD-08-ERD-062), LLE (414090-G), the Fusion Science Center at University of Rochester (412761-G), and GA (DE-AC52-06NA27279).

\* Also at Department of Mechanical Engineering, and Physics and Astronomy, University of Rochester.

[1] J. D. Lindl, *Inertial Confinement Fusion* (Springer-Verlag, New York 1999).  
 [2] S. Atzeni and J. Meyer-Ter-Vehn, *The Physics of Inertial Fusion* (Clarendon Press, Oxford 2004).  
 [3] R. P. Drake, *High-Energy-Density Physics* (Springer Press, New York, 2006).  
 [4] B. A. Remington *et al.*, *Science* **284**, 1488 (1999).  
 [5] L. J. Suter *Phys. Rev. Lett.* **73**, 2328 (1995).

[6] M. D. Rosen *et al.*, *Phys. Rev. E* **72**, 056403 (2005).  
 [7] M. Vandenboomgaerde *et al.*, *Phys. Rev. Lett.* **99**, 065004 (2007).  
 [8] P. A. Amendt *et al.*, *Phys. Plasmas* **15**, 012702 (2008).  
 [9] S. H. Glenzer *et al.*, *Phys. Rev. Lett.* **87**, 045002 (2001).  
 [10] S. I. Braginskii, *Review of Plasma Physics 1* (Consultants Bureau, New York, 1965).  
 [11] M. G. Haines, *Phys. Rev. Lett.* **78**, 254 (1997).  
 [12] C. K. Li *et al.*, *Phys. Rev. Lett.* **97**, 135003 (2006).  
 [13] M. M. Marinak *et al.*, *Phys. Plasmas* **5**, 2275 (2001).  
 [14] J. M. Soures, *et al.*, *Phys. of Plasmas* **3**, 2108 (1996).  
 [15] F. H. Séguin *et al.*, *Rev. Sci. Instrum.* **74**, 975 (2003).  
 [16] D. D. Meyerhofer *et al.*, *Phys. Plasmas* **8**, 2251 (2001).  
 [17] J. R. Rygg *et al.*, *Science* **319**, 1223 (2008).  
 [18] C. K. Li *et al.*, *Phys. Rev. Lett.* **100**, 225001 (2008).  
 [19] G. B. Zimmerman and W. L. Kruer, *Comm. in Plas. Phys. and Contr. Fus.* **2**, 51 (1975).  
 [20] C. K. Li *et al.*, *Phys. Plasmas* **7**, 2578 (2000).  
 [21] An asterisk structure similar in character to that described herein were observed, though not explicitly nor quantitatively discussed, from Au plasma x-ray self-emission in Nova 5-beam drive hohlraum experiments [22].  
 [22] S. H. Glenzer *et al.*, *Phys. of Plasmas* **6**, 2117 (1999).  
 [23] C. K. Li *et al.*, *Phys. Rev. Lett.* **99**, 015001 (2007).  
 [24] V. L. Highland, *Nucl. Instrum. Methods* **129**, 497 (1975).  
 [25] C. K. Li and R. D. Petrasso, *Phys. Rev. Lett.* **70**, 3059 (1993).  
 [26] The possibility that the proton depletion in the asterisk spokes could be due to  $E$  fields in the Au plasma jets (which requires  $\sim 10^9 \text{ V m}^{-1}$ ), rather than scattering in the jets, cannot be experimentally excluded by comparing measured deflections of protons at 3.3 and 15 MeV because the energy scaling is the same for both effects. But direct evidence for scattering is strong: the 3.3-MeV protons that passed through the spokes had lower energies than those passing between the spokes by  $\sim 40 \text{ keV}$ , which is consistent with the  $1 \text{ mg cm}^{-2}$  of Au required to generate the spokes through scattering. (the imaging detector has energy resolution [12,15]).  
 [27] With the separation between the electrons and ions on the order of a Debye length ( $\lambda_D$ ), and an ion inertial response on the order of an ion plasma frequency ( $\omega_{pi}$ ), a representative speed is obtained:  $C_s = \lambda_D \omega_{pi}$ .